J Therm Anal Calorim (2009) 96:697–704
DOI 10.1007/s10973-009-0020-9

Inter and intra-molecular branching distribution of tailored LLDPEs inferred by melting and crystallization behavior of narrow fractions

Madhavi Vadlamudi · Rufina G. Alamo · David M. Fiscus · Manika Varma-Nair

NATAS2008 Conference

Abstract Here we report the melting and isothermal crystallization behavior of two sets of fractions obtained from a film-grade metallocene catalyzed ethylene-1-hexene resin with enhanced mechanical properties. One set of fractions was obtained by molecular weight fractionation, the second set was obtained fractionating by content of 1-hexene. The melting behavior, crystallization kinetics and supermolecular morphology of the fractions are analyzed in reference to the behavior of model systems with uniform inter-chain branching content and a random intra-chain distribution. While melting and crystallization kinetics of molecular weight fractions conforms to the bivariate (molecular weight-comonomer content) distribution of the original copolymer, the behavior of 1-hexene compositional fractions indicate a blockier branching distribution in the highly branched high molar mass fractions. Major differences with model random copolymers are also observed in the supermolecular morphology of the latter fractions.

Keywords Ethylene copolymers · Bivariate distribution · Branching distribution · Crystallization kinetics · Ethylene 1-hexene

M. Vadlamudi · R. G. Alamo (✉)
Department of Chemical and Biomedical Engineering, FAMU/FSU College of Engineering, 2525 Pottsdamer St, Tallahassee, FL 32310, USA
e-mail: alamo@eng.fsu.edu

D. M. Fiscus
ExxonMobil Chemical Co, 5200 Bayway Drive, Baytown, TX 77522, USA

M. Varma-Nair
ExxonMobil Research and Engineering Co, Rt 22 East, Annandale, NJ 08801, USA

Introduction

The polyolefin industry has undergone a rapid revolution during the last two decades due to exponential advances in coordination catalysis that at the present time allow tailoring molecular microstructures with unique performances [1]. Linear low density polyethylenes (LLDPEs) can be obtained with a large variety of metallocene-type catalysts in homogeneous or heterogeneous processes, and are synthesized with a wider spectrum of comonomers than those feasible for copolymerization by the classical Ziegler-Natta catalysts. These novel metallocene catalysts provide independent control of molecular weight and comonomer composition distributions, while copolymers obtained with Ziegler Natta (ZN) catalysts invariably have tight relationships between the molar mass and the comonomer content. In the latter the highest concentration of comonomer is incorporated in the low molecular mass chains.

Although single-site metallocene catalysts lead to well controlled LLDPEs microstructures with unimodal narrow molecular mass and narrow inter-chain comonomer composition, processability suffers as the average molecular mass is increased to improve physical properties performance. This processing limitation was alleviated by engineering bimodal resins, a technology much improved in the last decade shifting from an initial blending to the use of tandem reactors and, ultimately to synthesizing tailored microstructures in a single reactor process [2]. Furthermore, tear and impact resistance are known to increase when the comonomer is preferentially incorporated in the high molar mass portion of the distribution [3]. Therefore, in addition to a bimodal molecular mass distribution, LLDPEs with enhanced properties often display a bimodal distribution of the content of comonomer that is orthogonal to the distribution given by ZN catalysts. It is perceived

that molecular connectivity between crystallites (tie molecules) increases, a key factor for enhanced mechanical properties of the film-grade resins [3].

A recent gas-phase process to produce LLDPEs with superior process/properties balance was described [4]. The copolymers have broad molecular mass distribution and broad complex comonomer composition distribution, where the content of comonomer increases with increasing molecular weight. One of these copolymers is the subject of study in this work. Fractions from this resin were obtained first by molecular mass and by comonomer content in a second fractionation to ascertain the details of the bivariate (molecular mass-comonomer composition) distribution from the GPC and TREF distribution profiles for each fraction. The advantage of collecting individual fractions, over automated methods of characterizing the cross-distribution [5] is that physical and morphological properties of the individual fractions can be studied in reference to the behavior of model narrow random copolymers. In this manner, the inter-chain comonomer composition can be inferred by a comparative melting and crystallization behavior of the molecular weight fractions with the model systems, while an analogous study with compositional fractions will probe the intra-chain comonomer distribution.

Experimental part

The parent ethylene 1-hexene copolymer studied was synthesized in a commercial gas-phase Unipol-type reactor using a metallocene catalyst [4]. The whole resin was fractionated by molecular mass into 10 fractions using a solvent/non-solvent fractionation technique at 130 °C with xylene/diethylene glycol monobutyl ether as solvent/non-solvent pair (M fractions) [6]. A set of 11 comonomer composition fractions was also obtained using preparative temperature rising elution fractionation (TREF) with ortho-dichloro benzene (o-DCB) as elution solvent, stabilized with 300 ppm of BHT (T fractions) [7]. The 0.4 g/100 cc solution was dissolved at 160 °C, subsequently stabilized at 95 °C, and slowly cooled from 95 to −20 °C at a rate of 0.5 °C/min. In a second step TREF fractions were collected raising the temperature in a range from −20 to 120 °C. Data for molecular characterization of the fractions are listed in Table 1.

The distribution and average molecular weights of the whole polymer and both sets of fractions were determined by standard Gel Permeation Chromatography (GPC) and the average comonomer composition was obtained using solution ^{13}C NMR. TREF profiles were obtained for each individual M or T fraction. The elution temperatures of these profiles are directly correlated with the inter-chain comonomer composition distribution. Dynamic crystallizations and further melting were followed by DSC at 10 °C/min using a Perkin Elmer DSC-7 with Pyris software, operating under nitrogen flow. The DSC was calibrated for static temperature and thermal lag effects with indium and connected to an intracooler to maximize heat transfer and to allow sub-ambient temperature control. The isothermal development of crystallinity with time was obtained from the exothermic crystallization peaks using differential scanning calorimetry (DSC). The initial fractions were pressed into ∼0.3 mm thin films between Teflon sheets at ca. 150 °C in a Carver press. About 4 mg of each film were encapsulated in aluminum pans and heated up to 180 °C for 3 min. Subsequently, the samples were cooled at 40 °C/min to the desired crystallization temperature (Tc) and held at this temperature until the heat flow returned to the initial baseline value. At this time the transformation was taken as complete. The overall crystallization rate was associated with the inverse of the time required to obtain half of the total transformation. The

Table 1 Molecular weight and NMR branching data of the whole ethylene 1-hexene initial resin and fractions. M–F# refers to molecular weight fractions and T–F# refers to TREF fractions

Fraction ID	Mn (g/mol)	Mw (g/mol)	Mw/Mn	Branch points (mol%)
Molecular weight fractions				
Parent resin	34000	123000	3.6	1.66
M-F1	5800	10000	1.8	1.42
M-F2	13000	18000	1.4	0.89
M-F3	23000	35000	1.5	1.13
M-F4	33000	48000	1.5	1.34
M-F5	51000	86000	1.7	1.57
M-F6	68000	118000	1.7	1.73
M-F7	92000	156000	1.7	1.78
M-F8	112000	187000	1.7	1.81
M-F9	147000	234000	1.6	1.81
M-F10	226000	336000	1.5	1.74
Comonomer composition fractions				
Parent resin	34000	123000	3.6	1.66
T-F1	15000	231000	15.4	5.48
T-F2	44000	249000	5.7	3.53
T-F3	19000	169000	8.8	3.14
T-F4	30000	207000	6.8	2.85
T-F5	37000	170000	4.6	2.10
T-F6	27000	131000	4.8	1.61
T-F7	24000	95000	3.9	1.13
T-F8	24000	70000	2.9	0.76
T-F9	24000	59000	2.5	0.52
T-F10	26000	57000	2.2	0.44
T-F11	31000	61000	1.9	0.46

enthalpy of fusion was calculated from the area of the melting endotherms and converted to the degree of crystallinity, $(1 - \lambda)_{\Delta H}$, by taking the enthalpy of fusion of a perfect polyethylene crystal to be 288×10^{-3} KJ g^{-1} [8].

Films for supermolecular morphological studies were prepared following the same melt-press method to reach ca. 50 μm thickness. Optical micrographs were obtained between crossed polarizers at room temperature using an Olympus BH-2 optical microscope equipped with an Olympus DP/2 digital camera and a Linkam hot stage TP-93. The temperature is controlled with a precision of ±0.1 °C. The film was placed between two microscope cover slips and heated to 150 °C for 3 min to eliminate any crystalline memory. Subsequently the temperature was lowered at a rate of 40 °C/min to the crystallization temperature (Tc), and allowed to reach the maximum crystallinity level at this Tc. Images were recorded at the Tc and after the crystallized film was taken at room temperature.

The small-angle light scattering patterns were obtained with an instrument described previously [9]. The H_v pattern was recorded. The radius of the spherulites was calculated from the following equation:

$$U_{\max} = \frac{4\pi R}{\lambda}\left(\sin\frac{\theta_{\max}}{2}\right) \quad (1)$$

In Eq. 1 U_{max} is the maximum scattering in the radial direction (= 4.1), R is the spherulitic radius, λ is the wavelength of radiation, 632 nm, and θ_{max} is the angle at which maximum scattering occurs.

Results and discussion

Bivariate distribution and melting behavior

A detailed characterization of the 1-hexene composition distribution across the molecular mass distribution (bivariate distribution) was first obtained from the gel permeation chromatography (GPC) and temperature rising elution fractionation (TREF) profiles of each M or T fractions, in a similar manner to other characterization works [5]. Using spline interpolation for data smoothing, a combination of these profiles proportionally to the weight fraction of each M or T fraction obtained, results in the molecular mass-comonomer composition distribution (the bivariate distribution). The independent bivariates obtained for M fractions or for T fractions are very similar. Shown in Fig. 1 are two 3-D views of the average distribution from both bivariates and their corresponding surface contour plots. The x and y-axes of these plots are respectively the log of molecular mass from the GPC profile and the temperature at which molecules are eluted during TREF characterization of each fraction. This temperature is inversely proportional to the comonomer content in the chain because molecules with low comonomer content form thick crystallites that are dissolved at the highest temperatures [7, 10]. As the comonomer content increases, the crystallites formed are thinner, thus dissolving at progressively lower temperatures. The bivariate distribution of the copolymer shows two major contours; about half of the mass of the initial resin are molecules with a relative low comonomer content that elute in a narrow elution temperature range (95 ± 2 °C). The chain length range of these molecules is very broad as seen by the large tails in the molar mass axis of this contour. The other half by mass of the distribution (second contour) corresponds to molecules that are broad in l-hexene composition and relatively narrower in chain length than the molecules with low comonomer content. According to this bivariate distribution it is expected that most molecular weight fractions will have molecules in both compositional contours, thus leading to a bimodal averaged crystallite thickness distribution. We estimate the comonomer content of molecules in the first low 1-hexene contour at approximately 1 mol%, and those in the second ranging between 1.5 and 11 mol%. Consequently, a bimodal melting behavior is expected for M fractions, as the l-hexene content from both contours is rather different. On the other hand, individual TREF fractions are narrow in composition and provided they have a random intra-chain distribution of the comonomer, their melting and

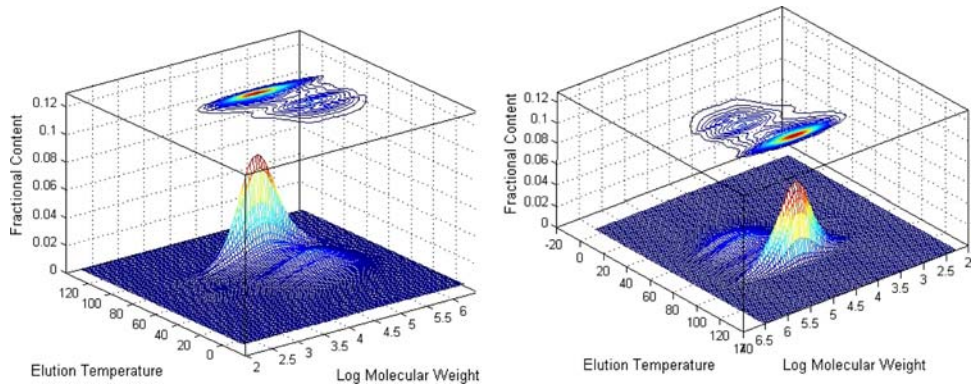

Fig. 1 Two side views and surface contours of the averaged 3-D bivariate (molecular mass-1-hexene content) distribution from GPC and TREF data corresponding to M and T fractions listed in Table 1. The profile on the right corresponds to a 180° rotation over the vertical axis of the left hand side profile

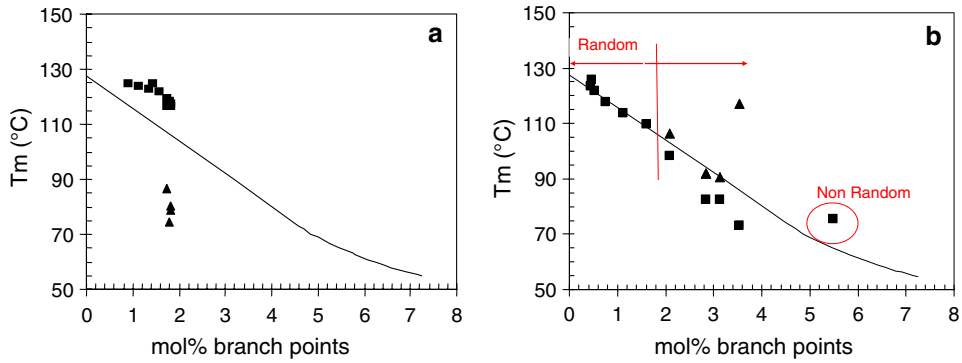

Fig. 2 Variation of the melting peak with mol% of branch points. **a** M fractions, **b** T fractions. Squares and triangles denote bimodal melting. The continuous lines represent the melting behavior of model random ethylene 1-alkene copolymers (ethyl and longer branches) extracted from Refs. [11–16]

crystallization behaviors should conform to the behavior of model copolymers already described [11–15].

We analyze the melting behavior of both sets of fractions in Fig. 2 where the peak melting temperatures are plotted vs mol percent of butyl branches obtained by ^{13}C NMR for M (Fig. 2a) and T (Fig. 2b) fractions respectively. Indeed, most M fractions display two melting peaks in agreement to the bivariate distribution, one above and the second below the melting value corresponding to narrowly distributed fractions of the same branching content. Melting for the latter are taken from previous literature data and are represented by the continuous line in this figure [11, 15]. The peaks in the 115–125 °C range correspond to crystallites formed from the low l-hexene content contour and those in the 70–90 °C range are crystals from molecules in the higher l-hexene content contour. Thus, this copolymer contains high molar mass chains with both low and high l-hexene content that may be responsible for the enhanced properties.

The melting behavior of T fractions is given in Fig. 2b. The melting of fractions with $<\sim 2$ mol% branching falls on the line of the random models. From this analysis we conclude that these low branched molecules have a random comonomer distribution. However, the melting behavior of fractions with >2 mol% is multi-peaked and deviates upward from the random line for the fraction with the highest branching content. We conclude from these data that the intra-chain distribution of the highly branched molecules deviates from the random pattern.

The crystallinity values obtained from the heat of fusion for M and T fractions are shown in Fig. 3a and b, respectively. By analogy with Fig. 2, the continuous line represents the behavior of model copolymers extracted from a previous works [15]. We notice that due to the bimodal branching composition, the total crystallinity of M fractions does not give the expected value for the narrow copolymers of the same branching composition. Depending on the relative weight fraction of lowly or highly-branched chains, the crystallinity content of the M fractions is above or below the line of the model copolymers or below this line. T-fractions follow the crystallinity pattern of the random model samples except for the highly branched fractions that have lower values as a consequence of their high molar mass and their blockier intra-chain distribution.

Crystallization kinetics

Isothermal crystallization kinetics of M and T fractions were studied comparatively with model copolymers of matched branching composition as an additional test to probe the inter- and intra-chain branching distributions of these fractions. The molecular and branching characterization data of samples studied are listed in Table 2. Samples labeled EH are narrowly distributed ethylene 1-hexenes synthesized with metallocene catalysis in a homogeneous process. These are the same copolymers studied in our previous works [12, 15]. Samples labeled

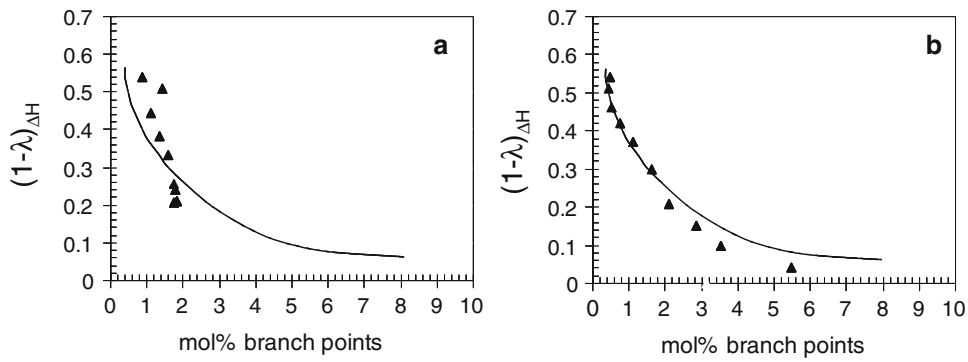

Fig. 3 Variation of the crystallinity fraction with mol% of branch points. **a** M fractions, **b** T fractions. The continuous lines represent the behavior of model random ethylene 1-alkene copolymers (ethyl and longer branches) extracted from Refs. [11–16]

Table 2 List of M or T fractions and matched model copolymers

Sample	Mw (g/mol)	Mw/Mn	Branch points (mol%)
M-fractions and model analogs			
Model EH 1.40	54000	2.1	1.40
M-F4	48000	1.5	1.34
M-F5	86000	1.7	1.57
Model HPBD 2.1	108000	1.3	2.10
M-F7	156000	1.7	1.78
M-F9	234000	1.6	1.81
T-fractions and model analogs			
Model EH 0.60	56000	2.1	0.60
T-F9	59000	2.5	0.52
Model EH 1.40	54000	2.1	1.40
T-F6	131000	3.5	1.61
Model HPBD 2.1	108000	1.3	2.10
T-F5	170000	5.7	2.10
Model HPBD 4.14	98000	1.1	4.14
T-F2	249000	5.7	3.53

HPBD are hydrogenated polybutadienes, analogous to ethylene 1-butene copolymers. It has been proven that EH and HPBD copolymers have uniform inter-chain branching composition and the random intra-chain distribution [11, 12, 15, 16].

The natural log of the overall crystallization rate, defined as the inverse of the time required to obtain half of the maximum crystallinity ($1/t_{0.5}$) is plotted vs crystallization temperature in Fig. 4 for representative M fractions and their model analogs. For all M fractions the range of temperatures where isothermal crystallization can be experimentally followed is 10–20° higher than for the model samples, clearly indicating that the crystallization rate of the M fractions is higher, and led by the lowly branched molecules, as expected for fractions with a bimodal branching composition.

The comparative overall crystallization rate data of T-fractions and model copolymers are shown in Fig. 5. Data for copolymers with <2 mol% branches are shown in Fig. 5a and those with >2 mol% branch points are given in Fig. 5b. In agreement with the melting results discussed above, the crystallization rate behavior of T-F9 and T-F6 is basically the same as their model counterparts, EH-0.6 and EH-1.4. These data give additional evidence for the random intra-molecular branching distribution of the lowly-branched T-fractions. Conversely, as shown in Fig. 5b, the crystallization of T-fractions of >2 mol% can only be experimentally followed in a higher temperature range, indicating that for the same crystallization temperature (Tc) T-fractions crystallize faster than the random models with matched composition.

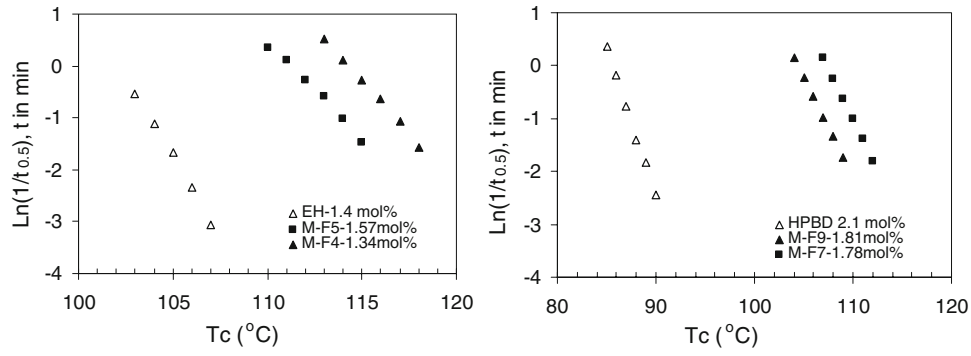

Fig. 4 Comparison of overall crystallization rates of M fractions and model copolymers with matched branching composition. Left, fractions with ~1.4 mol% branches. Right, fractions with ~2 mol% branches. Filled symbols are data for M-Fractions and open symbols for model copolymers

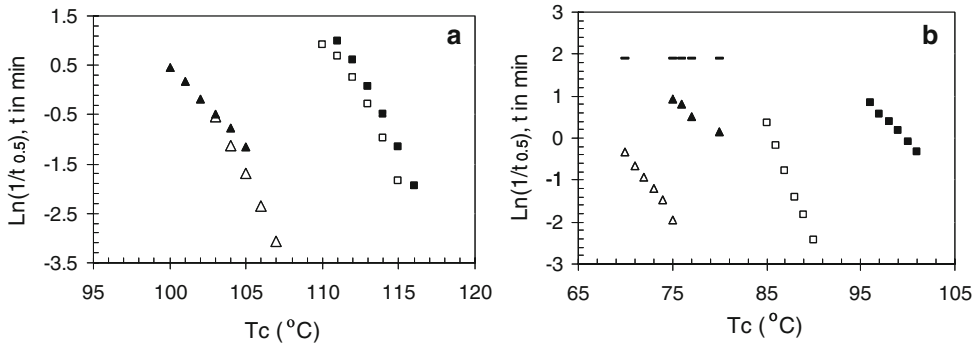

Fig. 5 Comparison of overall crystallization rates of T fractions and model copolymers with matched branching composition. **a** T-F9/EH-0.6 (*squares*), and T-F6/EH-1.4 (*triangles*). **b** T-F5/HPBD-2.1 (*squares*), and T-F2/HPBD-4.14 (*triangles*) (see text for explanation of dash and *filled triangles* for T-F2). Filled symbols are data for T fractions and open symbols for model copolymers

All T-fractions have uniform inter-chain l-hexene content, similar to their model counterparts, as the fractionation is based on comonomer composition. Therefore, the difference in rates must be associated with a different intra-chain branching distribution. The observed higher crystallization rates of highly branched T-fractions are associated with the presence of ethylene runs longer than the expected length for the random distribution. This suggests a blockier intra-chain distribution of the comonomer in the highly branched, high molecular mass chains of this resin. This interpretation is based on a sequence length-based selection mechanism of ordering of random copolymers with one of the units rejected from the crystalline regions. During isothermal crystallization, the crystalline ethylene runs are partitioned into crystallites according to their length [17, 18]. The longest sequences are selected earlier in this process. This explains the faster rates of T-fractions >2 mol% with a blocky-type distribution. At a matched composition these fractions have fast-crystallizing ethylene runs longer than any ethylene run of the model analogs. Furthermore, T-F2 (with ~3.53 mol% branches) displays two crystallization peaks, one is fast and invariant with Tc, typical of the behavior of blocky distributions (shown by the bar symbol in Fig. 5b), the second appears at longer times with increasing temperature (*filled triangles* in this figure). Both exotherms correspond to higher rates compared to the model hydrogenated polybutadiene (HPBD 4.14). Hence, all the crystallization rate data point to a branching micro-structure for these molecules with long ethylene crystalline sequences as was inferred from the melting behavior. The intra-chain 1-hexene distribution of the highly branched, high molecular weight fractions deviates strongly from the random behavior, i.e., chains rich in l-hexene content posses a blocky branching distribution while lowly-branched molecules are randomly distributed.

Supermolecular Morphology

The supermolecular morphology of the fractions observed by polarized optical microscopy (OM) and by small angle laser light scattering (SALS) was also compared with model copolymers for the samples listed in Table 2. Figure 6 gives OM images of M-F9 (1.81 mol%) and HPBD-2.1 mol% obtained at the same isothermal crystallization temperature before cooling (top row, Tc = 95 °C). The lower row displays OM and SALS images taken at room temperature after crystallization at 95 °C. The morphologies shown follow the spherulitic pattern observed for ethylene copolymers after isothermal crystallization [19, 20]. At the isothermal crystallization temperature only the low branched component of M-F9 crystallizes forming small spherulites similar to those developed by the random HPBD 2.1. A major difference is found after quenching at room temperature due to additional crystallinity. The amount of crystallinity that random copolymers of this nature develop, in addition to the transformation reached at the isothermal conditions, increases quite significantly during cooling. Crystallinity is increased because the short sequences having insufficient length to crystallize at the higher temperature crystallize at lower temperatures during the cooling process. We clearly see this effect by comparing the micrographs of the top and lower rows of Fig. 6. After quenching, due to the bimodal distribution of comonomer content, M fractions develop somewhat better organized spherulites than their random counterparts.

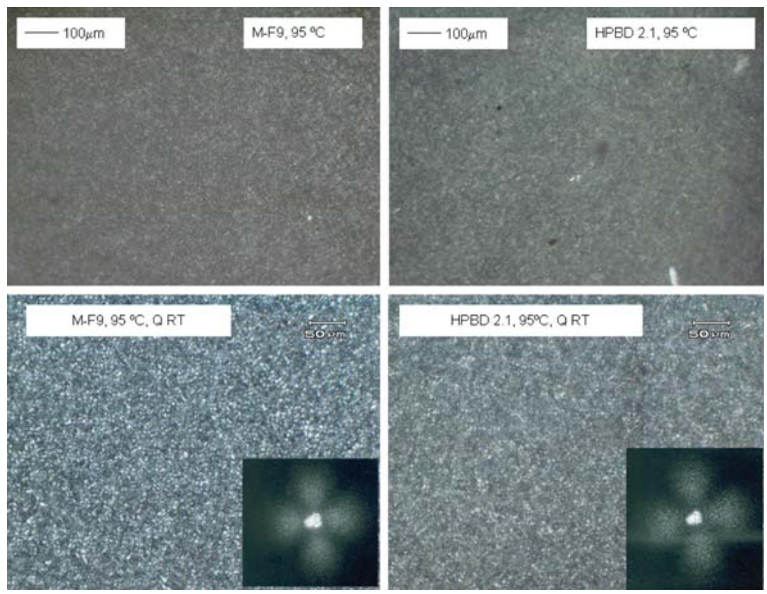

Fig. 6 Polarized optical micrographs of M-F9 (1.81 mol%) and HPBD-2.1 mol% crystallized at 95 °C. Optical micrographs and small angle laser light scattering (SALS) patterns of the same samples crystallized at 95 °C and quenched at room temperature

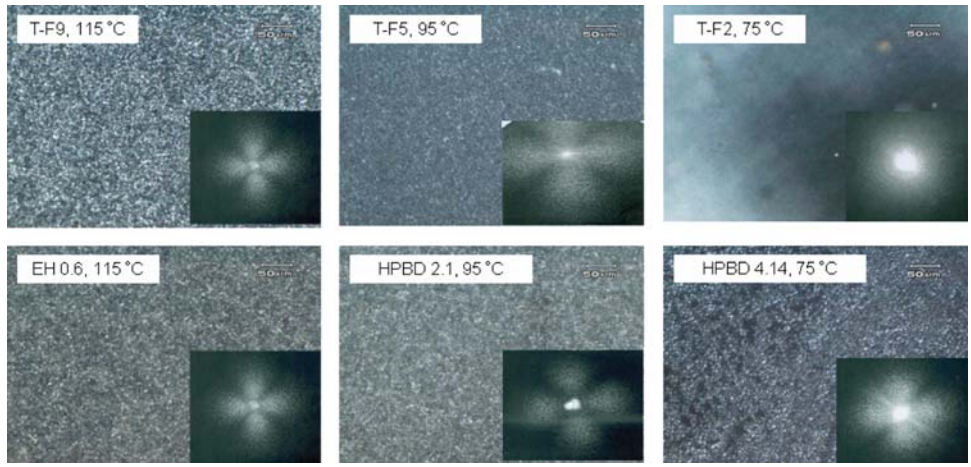

Fig. 7 Polarized optical micrographs and SALS patterns of T fractions (*top row*), and matched model copolymers (*lower row* of images) for samples quenched at room temperature after isothermal crystallization at the indicated temperatures

Table 3 Comparative supermolecular structures of M and T fractions and matched model copolymers

Sample	Microscope observations	SALS pattern	Radius of Spherulites, μm
M-fractions and model analogs			
Model EH 1.40 (Tc = 116 °C, Q to RT)	Spherulites	b type	3.73
M-F4 (Tc = 116 °C, Q to RT)	Spherulites	a type	4.21
Model HPBD 2.1 (Tc = 95 °C, Q to RT)	Spherulites	b type	3.34
M-F9 (Tc = 95 °C, Q to RT)	Spherulites	Between a and b type	3.94
T-fractions and model analogs			
Model EH 0.60 (Tc = 115 °C, Q to RT)	Spherulites	a type	4.21
T-F9 (Tc = 115 °C, Q to RT)	Spherulites	a type	4.21
Model EH 1.40 (Tc = 116 °C, Q to RT)	Spherulites	b type	3.73
T-F6 (Tc = 116 °C, Q to RT)	Spherulites	b type	3.73
Model HPBD 2.1 (Tc = 95 °C, Q to RT)	Spherulites	b type	3.34
T-F5 (Tc = 95 °C, Q to RT)	Very small spherulites	b type	0.77
Model HPBD 4.14 (Tc = 75 °C, Q to RT)	Disordered spherulites	c type	N/A
T-F2 (Tc = 75°C, Q to RT)	Faint areas of disordered objects	No pattern	N/A

OM images and SALS patterns taken at room temperature of isothermally crystallized T-fractions and model analogs are given in Fig. 7. There are minor differences in morphology between T-F9 and the random EH-0.60 as expected for matched copolymers with the same branching distribution. Both develop symmetric spherulites of the "a" type, according to the classification previously established [9, 21]. Differences in morphology between the fractions and the copolymers are found for copolymers >2 mol%, as shown in this figure. A consequence of the blockier distribution is a higher nucleation density of these T fractions compared with random analogs crystallized at the same temperature. A faster nucleation leads for T-F5 and T-F2 to small and defective supermolecular morphologies, while spherulites are developed by the random analogs. The major differences in supermolecular aggregates are found at the highest comonomer content. Spherulites are clearly distinguished for HPBD-4.14 mol%, while T-F2 develops faint objects with no distinctive pattern. A summary of the comparative morphologies, OM and SALS patterns, and the sizes of the spherulites is listed in Table 3.

Conclusions

The bivariate, molecular mass-comonomer composition distribution of a novel ethylene 1-hexene copolymer with enhanced mechanical performance over classical resins, indicates a unique and complex bimodal distribution of 1-hexene over the distribution of chain lengths. A detailed analysis of the melting behavior and overall crystallization rates of molecular weight fractions (M fractions) conforms to the bimodal comonomer composition of equal length chains, also found in the bivariate. This bimodal composition is responsible for the observed double melting of M fractions, and for their faster crystallization rates compared to the rates of copolymers with uniform inter-chain composition.

Thermal analysis of fractions obtained by extracting molecules with the same comonomer composition (T-fractions) is useful to infer the intra-molecular comonomer distribution. The intra-chain branching microstructure is not obtained from the bivariate distribution. In the resin studied, the comonomer of molecules with <2 mol% branching is randomly distributed. For these fractions the melting behavior and overall crystallization rates are identical to the data for model copolymers with uniform inter-chain composition and the random distribution. In contrast, chains with a high 1-hexene content (>2 mol%) display multiple melting peaks and faster crystallization rates than for matched random model copolymers, suggesting a comonomer distribution in these highly branched molecules that deviates from the random pattern. As a consequence, major differences are also observed in their comparative supermolecular morphologies. It is perceived that these microstructural features and the bimodal character of the composition distribution of this copolymer, that contains high molecular weight chains with both low and high 1-hexene contents, are responsible for the semicrystalline morphology that leads to enhanced film properties.

Acknowledgements We are indebted to the ExxonMobil Co. for financial support and clearance for publication of this work. The assistance of undergraduate student Belen Kelly is also acknowledged.

References

1. Chum PS, Swogger KW. Olefin polymer technologies-history and recent progress at the dow chemical company. Prog Polym Sci. 2008;33:797–819.
2. Liu H-T, Davey CR, Shirodkar PP. Bimodal polyethylene products from unipol (Tm) single gas phase reactor using engineered catalysts. Macromol Symp. 2003;195:309–16.
3. Krishnaswamy RK, Yang Q, Fernandez-Ballester L, Kornfield JA. Effect of the distribution of short-chain branches on crystallization kinetics and mechanical properties of high-density polyethylene. Macromolecules. 2008;41:1693–704.
4. McL Farley J, Szul JF, McKee MG. US Patent 6, 956, 088 (2005).
5. Ortin A, Monrabal B, Sancho-Tello J. Development of an Automated Cross-Fractionation Apparatus (TREF-GPC) for a full characterization of the bivariate distribution of polyolefins. Macromol Symp. 2007;257:13.
6. Holtrup W. Fractionation of polymers by direct extraction. Die Makromol Chem. 1977;178:2335–49.
7. Wild L. Temperature rising elution fractionation. Adv Polym Sci. 1990;98:1–47.
8. Quinn FA Jr., Mandelkern L. Thermodynamics of crystallization in high polymers - poly-(ethylene). J Amer Chem Soc. 1958;80:3178–82.
9. Maxfield J, Mandelkern L. Crystallinity, supermolecular structure, and thermodynamic properties of linear polyethylene fractions. Macromolecules. 1977;10:1141–53.
10. Soares JBP, Monrabal B, Nieto J, Blanco J. Crystallization analysis fractionation (Crystaf) of poly(ethylene-Co-1-octene) made with single-site-type catalysts: a mathematical model for the dependence of composition distribution on molecular weight. Macromol Chem Phys. 1998;199:1917–26.
11. Alamo RG, Domszy RC, Mandelkern L. Thermodynamic and structural-properties of copolymers of ethylene. J Phys Chem. 1984;88:6587–95.
12. Alamo RG, Mandelkern L. Thermodynamic and structural-properties of ethylene copolymers. Macromolecules. 1989;22:1273–77.
13. Alamo RG, Mandelkern L. Crystallization kinetics of random ethylene copolymers. Macromolecules. 1991;24:6480–93.
14. Alamo RG, Chan EKM, Mandelkern L, Voigt-Martin IG. Influence of molecular-weight on the melting and phase-structure of random copolymers of ethylene. Macromolecules. 1992;25:6381–94.
15. Alamo RG, Mandelkern L. The crystallization behavior of random copolymers of ethylene. Thermochim Acta. 1994;238:155–201.
16. Rachapudy H, Smith GG, Raju VR, Graessley WW. Properties of amorphous and crystallizable hydrocarbon polymers .3. Studies of the hydrogenation of polybutadiene. J Polym Sci Polym Phys Ed. 1979;17:1211−22.
17. Crist B, Howard PR. Crystallization and melting of model ethylene-butene copolymers. Macromolecules. 1999;32:3057–67.
18. Crist B, Williams DN. Crystallization and melting of model ethylene-butene random copolymers: thermal studies. J Macromol Sci-Phys. 2000;B39:1–13.
19. Mandelkern L, Maxfield J. Morphology and properties of low-density (branched) polyethylene. J Polym Sci Polym Phys Ed. 1979;17:1913–27.
20. Glotin M, Mandelkern L. Crystalline morphology of isothermally crystallized branched polyethylene. Macromolecules. 1981;14:1394–404.
21. Mandelkern L. Relation between properties and molecular morphology of semi-crystalline polymers. Discuss Faraday Soc. 1979;68:310–9.